Research Article | Vol. 12, No. 12 / 1 Dec 2021 / Biomedical Optics Express 7338
Biomedical Optics EXPRESS

Vernier effect assisted sucrose sensor based on a cascaded Sagnac interferometer with no-core fiber

YUANFANG ZHAO,[1] MANTHANGAL SIVANESAN ARUNA GANDHI,[2] QIAN LI,[2] ZHENGYONG LIU,[3,4] AND H. Y. FU[1,*]

[1]Tsinghua Shenzhen International Graduate School & Tsinghua-Berkeley Shenzhen Institute (TBSI), Tsinghua University, Shenzhen 518055, China
[2]School of Electronics and Computer Engineering, Peking University, Shenzhen 518055, China
[3]Guangdong Provincial Key Laboratory of Optoelectronic Information Processing Chips and Systems, School of Electronics and Information Technology, Sun Yat-sen University, Guangzhou 510275, China
[4]Southern Marine Science and Engineering Guangdong Laboratory (Zhuhai), Zhuhai 519000, China
*hyfu@sz.tsinghua.edu.cn

Abstract: We propose a sucrose concentration sensor by utilizing a fiber Sagnac interferometer with no-core fiber (SI-NCF) based on the Vernier effect. The Vernier effect is realized by introducing a single Sagnac interferometer (SI) with a similar free spectral range of SI-NCF. When the NCF is exposed to the external sucrose solution, the cladding state of NCF is changed, which induces the wavelength shift of the SI-NCF. The measured sucrose concentration sensitivity of a single SI-NCF is 2.97 nm/M, and the sensitivity can be improved to -13.84 nm/M with the assistance of the Vernier effect, which is 4.66 times of the single SI-NCF. The sensor has the advantages of high sensitivity, easy-fabrication and cost-effectiveness which can be applied in the field of the food industry, chemistry and agriculture.

1. Introduction

Sucrose is the main component of sugar, indicating that it is an important food and sweet condiment. In addition, sucrose is one of the important raw materials in the production of alcohol, yeast, citric acid, lactic acid, glycerol, alcohols, medicines, etc. [1,2]. Therefore, it is necessary to develop a sensitive and efficient method to measure sucrose concentration in food, industrial and biological samples [3,4]. Optic fiber sensors have been extensively studied due to their advantages of electro-magnetic immune, tiny structure and high sensitivity [5–7], such as surface plasmon resonance (SPR) fiber sensor [8,9], localized surface plasmon resonance (LSPR) fiber sensor [10–12], fiber Bragg grating-based sensor [13], whispering gallery mode (WGM) based fiber sensor [14] and fiber interferometer based sensor [15,16]. Recently optic fiber interferometer based sensors have attracted extensive attention to researchers including multimode interferometer (MMI) [17], fiber Sagnac interferometer (FSI) [18], Mach-Zehnder interferometer(MZI) [19], etc. However, the sensitivity of a single interferometer is relatively low, Vernier effect is introduced into the single interferometer to enhance the sensitivity of biochemical detection in recent years [20,21]. Jiang et al. demonstrate a dual-microfiber coupler(MFC) based on the Vernier effect to test glycerin solution and realize refractive index (RI) detection in a narrow RI range [22]; Chen et al. designed a double helix microfiber coupler with the assistance of the Vernier effect to measure salt solution and enhance the RI sensitivity [23]. These methods are both based on microfiber MMIs that require high accuracy, which increases the manufacturing difficulty. In this line, some researchers try to find an approach without utilizing microfiber [24,25]. Li et al. fabricated MZI and FPI respectively by utilizing fiber core-offset techniques and cascaded the two interferometers to realize glycerin solution detection [26]. However, the

#444620 https://doi.org/10.1364/BOE.444620
Journal © 2021 Received 30 Sep 2021; revised 27 Oct 2021; accepted 28 Oct 2021; published 8 Nov 2021

Biomedical Optics EXPRESS

generation of Vernier effect generally requires two interferometers with similar free spectral range (FSR) and extinction ratio (ER), which indicates that the fabrication of two interferometers on optic fiber with a micro/nanostructure is still not easy.

Among all of the interferometers, Sagnac interferometer (SI) with polarization maintaining fiber (PMF), one of the stable and easy-fabricated interferometers, could generate regular interference spectra and is convenient to control the FSR and ER by adjusting the PMF length, polarization state and coupling ratio, which is easy to generate Vernier effect by cascading or parallel other interferometers. It has been used in various sensing applications, such as temperature sensor, RI sensor [27], magnetic sensor based on Faraday rotation [28], hydrogen sensor [29]. While for the biochemical analyst detection, as we mentioned before, the light is needed to leak out from the fiber, and a piece of fiber in SI should be tapered, fabricated micro/nano-structure or taken off the cladding part by corrosion method that is a complex and challenging to control the accuracy. In addition, the mechanical strength of the whole structure after the treatment above also decreases, which is not a good choice for sensing applications. No-core fiber (NCF) is a kind of silica fiber with the same refractive index (RI) in core and cladding parts. Due to no RI difference in NCF, the external substance can serve as the "cladding" of NCF and seldom need tapering and chemical corrosion which is favorable for the optic fiber biochemical sensor [30]. Therefore, the NCF is gradually introduced into the optic fiber sensors [31]. Xiao et al. use graphene oxide coated single-mode fiber (SMF)-NCF-SMF (SNS) structure to measure sucrose solution with a refractive index of 1348.67 nm/RIU in an ultra-narrow RI range of 1.33-1.3385 [32]. However, the work above needs special material to sensitize the sensor which increases the fabrication complexity. Therefore, inserting NCF into SI can realize the leakage of light and realize direct interaction of the analyst liquid, which is a benefit for the biochemical sensing application of SI. Meanwhile, cascading a SI onto the single interferometer to introduce the Vernier effect will enhance the sensitivity indeed without modifying special material.

In this work, we propose and demonstrate a Sagnac interferometer with no-core fiber (SI-NCF) based on the Vernier effect for sucrose concentration detection. By sensor calibrating, the most suitable length of NCF is determined. Then we cascade an ordinary Sagnac interferometer (SI) into the SI-NCF to produce the Vernier effect and enhance the sensor performance. The experiment results show that the relationship between the wavelength shift and sucrose is linear. And the sensitivity of the sucrose concentration to wavelength shift is 2.97 nm/Mol/L. After cascading the reference arm onto the sensor arm, the sensitivity can be increased to -13.84 nm/Mol/L which is 4.66 times the single one. The sensor can be widely used in chemistry, food, pharmaceutical, agriculture and other fields due to its advantages of high sensitivity, simple manufacture and cost-effectiveness.

2. Experimental setup and sensing principle

2.1. Experimental setup

Figure 1 shows the experimental setup of the proposed sucrose concentration sensor system. The light launched by a broadband optic light source (ASE, ALS-CL-15-B-FA, Amonics,) with 100 nm spectral bandwidth enters into the reference Sagnac interferometer (SI) after passing through a fiber isolator, and then the light is injected into Sagnac interferometer with no-core fiber (SI-NCF), finally, the interference spectra are observed and monitored by an optical spectrum analyzer (OSA, AQ6370D, YOKOGAWA). To eliminate the temperature perturbation from an ambient environment, we put the sensor part onto a thermostat to keep the temperature unchanged and increase the sensor's stability. The reference SI consists of a 3-dB coupler, a section of PMF and a polarization controller (PC). The sensor SI-NCF is constructed by inserting a section of NCF into a SI.

Biomedical Optics EXPRESS

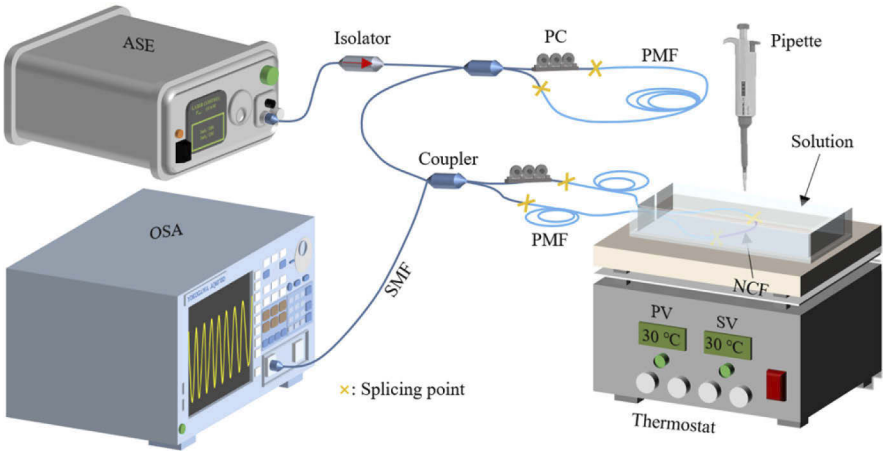

Fig. 1. Experiment set-up of the proposed sucrose sensor system.

2.2. Sensing principle

For the reference SI, it is an ordinary PMF Sagnac interferometer, the transmission can be expressed as [33]

$$I = \frac{(1 - cos(\varphi))}{2}, \tag{1}$$

where φ=(2·π·Δn·L)/λ is the phase shift, L and λ are the PMF length and the wavelength respectively, Δn is the birefringence of PMF. The FSR of reference SI can be derived as

$$FSR_{SI} = \frac{\lambda^2}{\Delta n \cdot L}. \tag{2}$$

For the sensor SI-NCF, its structure is divided into three sections as shown in Fig. 2(a), two sections of PMFs and one section of NCF. A section of no-core fiber (NCF) is inserted into the two portions of PMFs, and the external medium acts as the cladding of NCF. The interaction between sucrose concentration and NCF could change the interference state of the SI-NCF. When we cascade the SI-NCF sensor and the reference SI, the two interferometers with similar FSR will superimpose the two-interference spectrum and generate a bigger envelope. The FSR of the envelope can be expressed as [21],

$$FSR_{envelope} = \frac{FSR_{SI} \cdot FSR_{SI-NCF}}{|FSR_{SI} - FSR_{SI-NCF}|}, \tag{3}$$

where FSR_{SI-NCF} is FSR of the SI-NCF. Compared to a single SI-NCF sensor, the envelope shift of cascaded configuration can be magnified with an impact factor M,

$$\mathrm{M} = \frac{FSR_{SI}}{|FSR_{SI} - FSR_{SI-NCF}|}. \tag{4}$$

The sign of denominator $FSR_{SI} - FSR_{SI-NCF}$ determines the direction of wavelength shift. When the sign of $FSR_{SI} - FSR_{SI-NCF}$ is positive, the sensitivity curve's slope of NCF-SI with Vernier effect will not change. When the sign of $FSR_{SI} - FSR_{SI-NCF}$ is negative, the sensitivity curve's slope of NCF-SI with Vernier effect will change.

Biomedical Optics EXPRESS

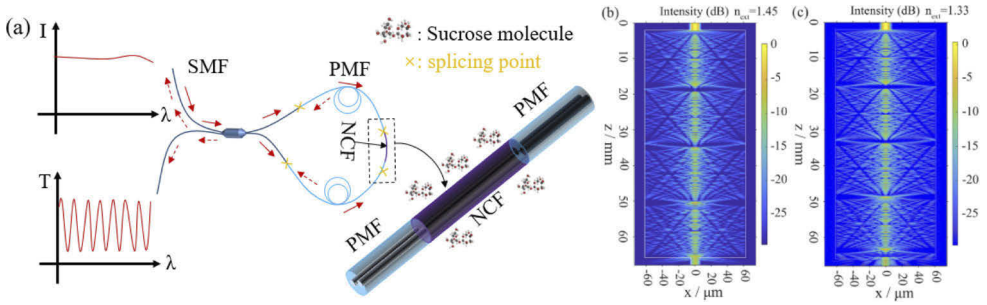

Fig. 2. (a) Schematic diagram of the designed sensor based on SI-NCF; The BPM simulation for intensity distribution of PMF-NCF-PMF: the RI around the NCF are 1.45(b) and 1.33(c) (here, the intensity are defined as I(x,z)/I(input) at y=0 μm).

2.3. Simulation analysis

To better understand the interaction between the external RI and the NCF, we use the beam propagation method (BPM) to simulate the PMF-NCF-PMF (PNP) part in SI-NCF. The basic simulated parameters are listed below. The two sections of PMF length are both 10 mm and the NCF length is 64 mm. The bi-refractive index, numerical aperture and diameter of PMF are 4.5×10^{-4}, 0.125 and 10 μm, respectively. The core refractive index and diameter of NCF are 1.4440 and 125 μm, respectively, external RI acts as the cladding RI of NCF. the simulated wavelength is 1550nm, the grid size is 150×150 μm^2, the grid points are 200×200. The simulated results are shown in Fig. 2(b-c). As one can observe, when light is transmitted in PMF, the energy is mainly confined in the core of PMF. When the light incidents from PMF to NCF, due to the core mismatch between the two kinds of fiber, multi-modes will be excited. Then, the excited multi-modes will interfere with each other during the light propagation. It is apparent that the periodic optic field distribution occurs in NCF part with a four-cycle of the self-imaging pattern is formed, which means mode interference exists in NCF. When we change the RI value of the "cladding part" from 1.45 to 1.33, even if the NCF length is the same, the size of each self-imaging pattern is changed with different RI of external substance. It indicates that the designed sensor could be used for biochemical analyst detection with different RI analytes.

3. Experiment results and discussion

3.1. Sensor calibration

First, we use a longer NCF to ensure sufficient contact between the solution and NCF. Under this condition, we studied the RI response of the sensor SI-NCF by immersing the NCF part into a different concentration of sucrose. The RI value of each sucrose solution is obtained by utilizing an Abbe refractometer. The corresponding RI value for sucrose solution of 0.1 Mol/L, 0.2 Mol/L, 0.3 Mol/L, 0.4 Mol/L, 0.5 Mol/L are 1.3380, 1.3431, 1.3482, 1.3532, 1.3590, accordingly. We keep the temperature around 28°C and keep the polarization state of the sensor stable and unchanged and then pipette an increased concentration of sucrose into the sensor part. The measured interference spectra of the SI-NCF with different RI are depicted in Fig. 3(a). It can be noticed that the resonance spectra have a redshift with the increasing of RI value. To evaluate the RI sensitivity of the SI-NCF sensor, one typical dip at 1549.2 nm is monitored and the dip values at different RI are given in Fig. 3(b). With the RI increasing from 1.3380 to 1.3590, the wavelength shift is 1.6 nm and the refractive index sensitivity is 46.68 nm/RIU. The linear fit coefficient is 0.986 with good linearity. To ensure the experimental accuracy, we carry out the measurement three times and take the mean value. The error bar shown in Fig. 3(b) is the standard deviation for the three repeated measurements. The mean-variance of all selected

Biomedical Optics EXPRESS

resonance wavelengths is 0.03 nm, which is relatively small. This result indicates the SI-NCF sensor is efficient to test solutions with different RI values.

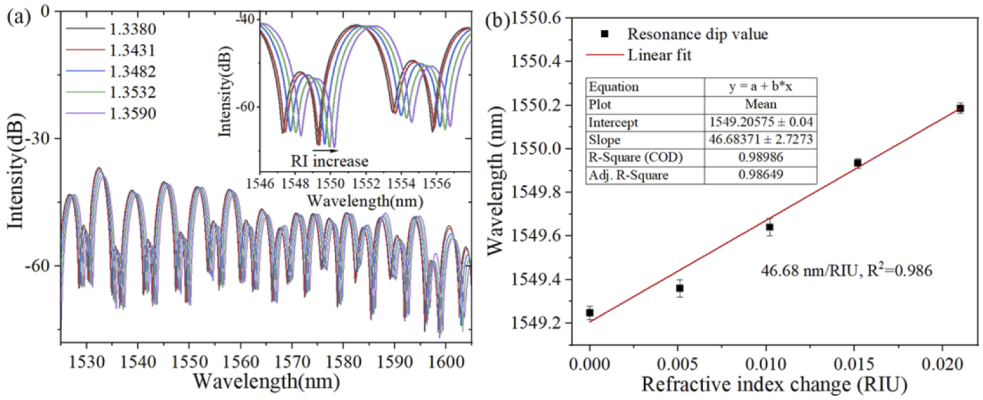

Fig. 3. (a) The interferometer spectra of the SI-NCF sensor without Vernier effect under RI increasing; (b) The corresponding relationships between the wavelength and refractive index of the single SI-NCF sensor.

The transmission spectra are shown in Fig. 3(a) and there are two small dip branches in one resonance dip, making the resonance spectra non-uniform. The non-uniform spectra of SI-NCF are caused by the interference between the two pieces of PMF and the multimode interference between NCF and PMF. The non-uniform spectrum is not suitable for the generation of the Vernier effect. However, we need uniform spectra to generate the Vernier effect for the subsequent experiment. To obtain the uniform interference spectrum of the SI-NCF sensor, it should eliminate the effect mentioned above. The interference between the two pieces of PMF can be reduced by adjusting the polarization state and fast axis angle between two PMFs [29]. The multimode interference can be decreased by using an NCF with length away from the integral multiple of the cycle length of an interference pattern [32]. Therefore, we change the NCF length to 40 mm. In the transmission spectra in Fig. 4(a) there are no branches in one resonance dip and the spectra are more uniform, the FSR near 1535 nm for the resonance spectrum is 3.4 nm, which is more suitable for the subsequent detection compared to the previous NCF length.

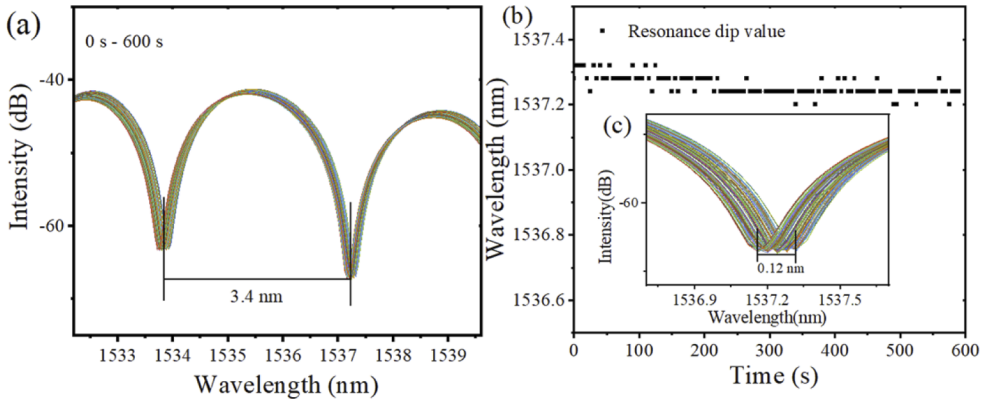

Fig. 4. (a) Measured resonance spectra with a time of single SI-NCF sensor; (b) Stability for the designed sensor; (c) The enlarge of the resonance dip at 1537.2 nm.

Biomedical Optics EXPRESS

When the NCF length is 40 mm, the interference spectra of SI-NCF are regular and uniform, thus we test the stability performance of the designed sensor by measuring the transmission spectra during a period under the temperature of 30℃. By tracking one of the resonance dips from the measured spectra as shown in Fig. 4(c), the stability result of the device was addressed in Fig. 4(b). From the figure, the tracked resonance dip keeps unchanged during 600 seconds and the wavelength dip variation is 0.12 nm wavelength range, which indicates the designed sensor has good stability. In conclusion, the designed SI-NCF sensor is suitable for the detection of sucrose with different concentrations with the assistance of the Vernier effect.

3.2. Result analysis

After the sensor calibration, we test the sucrose sensor performance of the single SI-NCF without Vernier effect using NCF with 40 mm length. Distilled water is injected into the sensor part to clean the container and the NCF. Then, five groups of sucrose solution with concentrations changed from 0.1 M to 0.5 M are prepared and sequentially pipetted onto the sensor part. Due to the change of external medium, the cladding composition of NCF is also changed, the resonance wavelength shifts occur. Figure 5(a) shows the measured resonance spectra with different sucrose concentrations. It indicates there is a redshift with an ascending concentration of sucrose concentration. Figure 5(b) gives the sensitivity characteristic of the sucrose sensor without the Vernier effect. The result shows there is a linear relationship between the wavelength shift and sucrose concentration in the current detection range and the sensitivity of the single SI-NCF sensor is 0.297 nm/Mm, with a linear correlation coefficient of 0.951. The single SI-NCF is robust and easy-fabrication, however, the sensitivity of single SI-NCF is relatively low which need further improved.

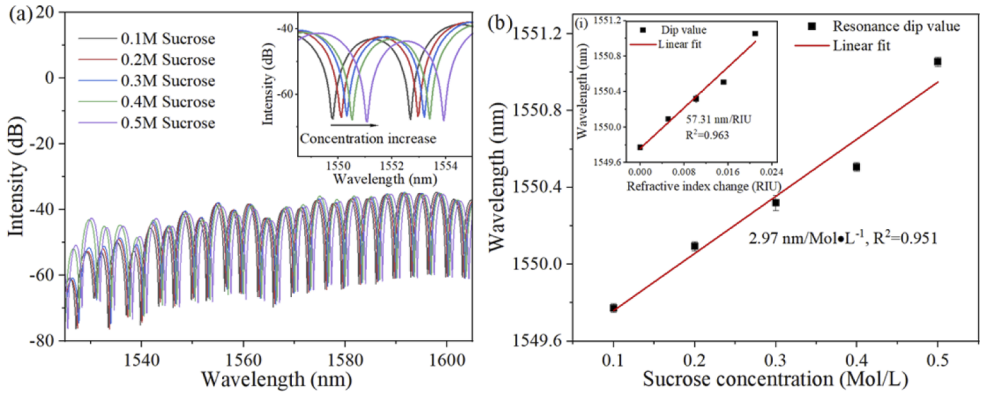

Fig. 5. (a) Measured resonance spectra with different sucrose concentrations for single SI-NCF sensor without Vernier effect; (b) the corresponding relationship between the resonance wavelength dip and the sucrose concentration (Inset (i): the corresponding relationship between the resonance wavelength dip and the RI).

3.3. Vernier effect

To improve the single SI-NCF's sensitivity, the Vernier effect is introduced into the SI-NCF sensor. Figure 6(a-b) exhibits the transmission spectrum of reference SI and sensor SI-NCF without Vernier effect, respectively. Both the extinction ratio (ER) of the two spectra is around 20 dB. In addition, the FSR of sensor SI-NCF near 1550 nm is 3.48 nm, while the FSR of reference SI near 1550 nm is 2.80 nm. The two spectra of sensor and reference have slightly free spectral ranges (FSRs) difference which look like two rulers with small scale difference. To enhance the sensor performance of the single SI-NCF sensor, a reference SI with similar

Biomedical Optics EXPRESS

FSR is cascaded onto the SI-NCF sensor to realize the Vernier effect. Figure 6(c) shows the transmission spectrum of cascading the reference SI and sensor SI-NCF with the Vernier effect. Compared with Fig. 6(a) and Fig. 6(b), the transmission spectrum of the cascaded configuration has a superimposed envelope, which is due to the similar FSR between the two interferometers. The envelope peak spacing is 14.28 nm, which is 4.10 times of the SI-NCF sensor, according to Eq. (4), indicating that it is promising to improve the SI-NCF sensor's sensitivity.

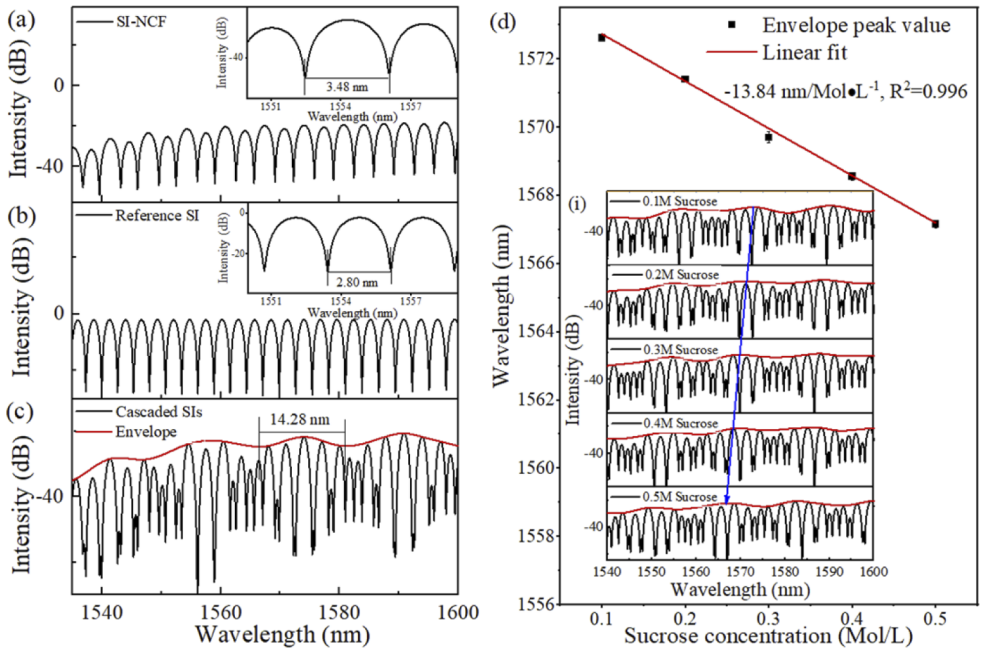

Fig. 6. (a) Measured resonance spectra of (a) single SI-NCF; (b) single reference SI; (c) the cascaded SI-NCF and reference SI. (d) the corresponding relationship between the resonance wavelength dip and the sucrose concentration for the cascaded SIs with Vernier effect (Inset (i): measured transmission spectra of the sucrose sensor based on Vernier effect with different concentration of sucrose)

Then, the sucrose solutions with different concentrations were delivered to characterize the sensor performance based on the Vernier effect according to the experimental setup as shown in Fig. 1. The inset figure in Fig. 6(d) shows the transmission spectra of the proposed sensor based on the Vernier effect at different sucrose concentrations. The envelope dips have a blue shift to 5.54 nm when the sucrose concentration increases from 0.1 M to 0.5 M. The blue shift is due to the FSR of reference SI being smaller than the FSR of sensor SI- NCF [21]. The relationship between the envelope shift and the sucrose concentration is given in Fig. 6(d). As we can see, the sucrose sensitivity is -13.84 nm/M, which is 4.66 times higher than the single SI-NCF sensor without the Vernier effect. The linear correlation coefficient is 0.996, which shows good linearity. In conclusion, without special material modified on NCF, cascading an easy-fabrication SI onto the sensor SI-NCF to realize the sensitivity amplification which is more convenient and cost effectiveness.

We compare the sucrose concentration sensitivity and RI sensitivity for the SI-NCF with the Vernier effect and without the Vernier effect respectively in Fig. 7. The values of the sensitivity and magnification coefficient are also listed in Table 1. As we can see, the sucrose concentration sensitivity of SI-NCF without the Vernier effect can be magnified 4.66 times by SI-NCF with the Vernier effect. The RI sensitivity of SI-NCF can be magnified 4.63 times with the assistance of

Biomedical Optics EXPRESS

the Vernier effect. The small difference in the magnification coefficient between the concentration sensitivity and RI sensitivity may come from the Abbe refractometer.

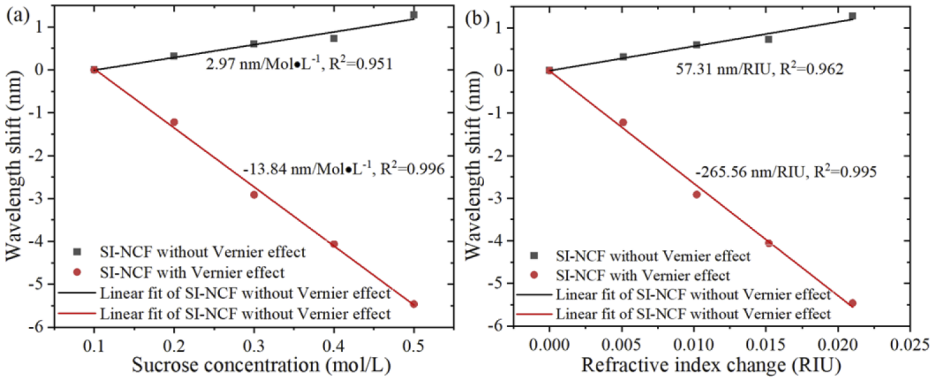

Fig. 7. The sensitivity comparison for the SI-NCF with Vernier effect and without Vernier effect: (a) Sucrose concentration sensitivity; (b) RI sensitivity.

Table 1. The comparison of the sensitivity for the SI-NCF with Vernier effect and without Vernier effect

Sensitivity	SI-NCF without Vernier effect	SI-NCF with Vernier effect	M
Concentration sensitivity	2.97 nm/(Mol/L)	-13.84 nm/(Mol/L)	4.66
RI sensitivity	57.31 nm/RIU	-265.56 nm/RIU	4.63

To compare the efficiency of the proposed sensor to the existing sensor, we summarize the performance comparison in Table 2. Hu et al. cascade an SMF-NCF-SMF (SNS) structure and a SI to realize the detection of NaCl solutions, the RI sensitivity is 96.42 nm/RIU which is relatively low [34]. To improve the sensitivity, Zhou et al. coated the microfiber with graphene oxide (GO) in SI and meanwhile utilized the Vernier effect to achieve a relatively high RI sensitivity of 2429 nm/RIU [27]. Li et al. proposed a SI with exposed core fiber (ECF) to realize a low detection limit refractive index sensing and the RI sensitivity is 2487 rad/RIU [35]. However, the sensor structure needs a microchannel which requires precision fabrication. Xiao et al. utilize GO coated SNS fiber structure and achieve a sucrose detection, the sensitivity can increase to 1348.67 nm/RIU with the GO sensitized [32]. Even though the SNS fiber structure is robust than other micro/nano fiber structures, the modification of GO will increase the manufacturing difficulties and the service life and sensitivity will also decrease with the damage of GO material under multiple detections of liquid. To replace the special material modified and sensitized the NCF sensor, we utilize a robust PMF-NCF-PMF structure in SI, meanwhile, employing an easy-fabricated reference SI to excite the Vernier effect to achieve the sensors' sensitivity amplification. The sucrose concentration sensitivity of our proposed sensor is -13.84 nm/(Mol/L),

Table 2. The performance comparison between the proposed sensor with the existing sensor

Structure	Material assisted	Detection RI range	RI sensitivity	year	Reference
SI and SNS fiber	no	NaCl solution	96.42 nm/RIU	2016	[34]
GO-SI-taper and SI	GO assisted	1.3320-1.3369	2429 nm/RIU	2018	[27]
SI and MZI with ECF	no	1.3320-1.3465	2487 rad/RIU	2019	[35]
GO-SNS fiber	Go assisted	1.330-1.3385	1348.67 nm/RIU	2020	[32]
SI and SI-NCF	no	1.3380-1.3590	-265.56 nm/RIU	2021	Our work

Biomedical Optics EXPRESS

corresponding to a RI sensitivity of -265.56 nm/RIU. In summary, compared to other sensors, the proposed sensor shows the comprehensive performance of robust, easy-fabrication and high sensitivity which make it competitive and cost-effective.

4. Conclusion

In conclusion, we propose and demonstrate a Sagnac interferometer with no-core fiber (SI-NCF) based on the Vernier effect for sucrose concentration detection. We optimize the transmission spectra of SI-NCF by adjusting the NCF length. The experiment result shows when the NCF length is 40 mm, the spectrum of SI-NCF has regular FSR and ER. Cascading an ordinary Sagnac interferometer (SI) with similar FSR and ER into the SI-NCF generates the Vernier effect. The experimental results show that the sensitivity of the sucrose concentration is 2.97 nm/Mol/L for the single SI-NCF sensor. After cascading the reference SI onto the SI-NCF, the maximum sensitivity is -13.84 nm/Mol/L and 4.66 times compared to the single one. The proposed method explores an SI-NCF sucrose sensor with the benefits of easy fabrication, good stability and cost-effectiveness, which is suitable for sucrose detection in food, agriculture and industry fields.

Funding. National Natural Science Foundation of China (61905096); Innovation Group Project of Southern Marine Science and Engineering Guangdong Laboratory (Zhuhai) (No.311021011); Science, Technology and Innovation Commission of Shenzhen Municipality (JCYJ20180507183815699).

Disclosures. The authors declare no conflict of interest.

Data availability. The data presented in this study are available on request from the corresponding author.

References

1. L. Yuan and X. Dong, "Study on detection methods for sucrose," Int. J. Curr. Res. Chem. Pharm. Sci. **3**(11), 43–46 (2016).
2. Z. Li, X. Wu, K. Tong, X. Jia, W. Li, and Q. Li, "Sucrose concentration sensor based on MoS2 nanofilm and Au nanowire array enhanced surface plasmon resonance with a graphene oxide nanosheet," J. Opt. Technol. **87**(1), 40–45 (2020).
3. F. Perez-Ocon, A. M. Pozo, J. M. Serrano, and O. Rabaza, "Continuous measurement with three-in-one plasmon sensor in sucrose solutions," IEEE Sens. J. **21**(5), 6280–6286 (2021).
4. A. Rakesh, G. Kumar, A. Bhatt, A. Kapoor, M. Paliwal, V. Tomar, and Gupta, "Lossy mode resonance based refractive index sensor for sucrose concentration measurement," IEEE Sens. J. **20**(3), 1 (2019).
5. N. Bidin, N. H. Zainuddin, S. Islam, M. Abdullah, F. M. Marsin, and M. Yasin, "Sugar detection in adulterated honey via fiber optic displacement sensor for food industrial applications," IEEE Sens. J. **16**(2), 299–305 (2016).
6. P. Zaca-Morán, J. P. Padilla-Martínez, J. M. Pérez-Corte, J. A. Dávila-Pintle, J. G. Ortega-Mendoza, and N. Morales, "Etched optical fiber for measuring concentration and refractive index of sucrose solutions by evanescent waves," Laser Phys. **28**(11), 116002 (2018).
7. P. Gong, X. Li, X. Zhou, Y. Zhang, N. Chen, S. Wang, S. Zhang, and Y. Zhao, "Optical fiber sensors for glucose concentration measurement: A review," Opt. Laser Technol. **139**, 106981 (2021).
8. S. K. Chauhan, N. Punjabi, D. K. Sharma, and S. Mukherji, "A silicon nitride coated LSPR based fiber-optic probe for possible continuous monitoring of sucrose content in fruit juices," Sens. Actuators, B **222**, 1240–1250 (2016).
9. F. Wang, M. Lu, H. Yuan, Y. Zhang, W. Ji, C. Sun, and W. Peng, "pM level and large dynamic range glucose detection based on a sandwich type plasmonic fiber sensor," J. Lightwave Technol. **39**(12), 3882–3889 (2021).
10. S. Kumar, R. Singh, B. K. Kaushik, N.-k. Chen, Q. S. Yang, and X. Zhang, "LSPR-based cholesterol biosensor using hollow core fiber structure," IEEE Sens. J. **19**(17), 7399–7406 (2019).
11. S. Kumar, R. Singh, Q. Yang, S. Cheng, B. Zhang, and B. K. Kaushik, "Highly sensitive, selective and portable sensor probe using Germanium-doped photosensitive optical fiber for ascorbic acid detection," IEEE Sens. J. **21**(1), 1 (2020).
12. L. Singh, R. Singh, B. Zhang, B. K. Kaushik, and S. Kumar, "Localized surface plasmon resonance based hetero-core optical fiber sensor structure for the detection of L-Cysteine," IEEE Trans. Nanotechnol. **19**, 201–208 (2020).
13. Q. Li, X.-l. Zhang, Y.-S. Yu, Y. Qian, W.-F. Dong, Y. Li, J. Shi, J. Yan, and H. Wang, "Enhanced sucrose sensing sensitivity of long period fiber grating by self-assembled polyelectrolyte multilayers," IEEE Trans. Nanotechnol. **71**, 335–339 (2011).
14. H. Wan, J. Chen, C. Wan, Q. Zhou, J. Wang, and Z. Zhang, "Optofluidic microcapillary biosensor for label-free, low glucose concentration detection," Biomed. Opt. Express **10**(8), 3929–3937 (2019).
15. R. Qi, L. Xia, N. Wu, Z. Yang, and T. Ruan, "High resolution measurement of refractive index with resistance to temperature crosstalk through an all fiber MZI-PMF structure," Sens. Actuators, A **302**, 111790 (2020).
16. B. H. Lee, Y. H. Kim, K. S. Park, J. B. Eom, M. J. Kim, B. S. Rho, and H. Y. Choi, "Interferometric fiber optic sensors," Sensors **12**(3), 2467–2486 (2012).

Biomedical Optics EXPRESS

17. J. Kang, J. Yang, X. Zhang, C. Liu, and L. Wang, "Intensity demodulated refractive index sensor based on front-tapered single-mode-multimode-single-mode fiber structure," Sensors) **18**(7), 2396–2405 (2018).
18. Q. Liu, L. Xin, and Z. Wu, "Refractive index sensor of a photonic crystal fiber Sagnac interferometer based on variable polarization states," Appl. Phys. Express **12**(6), 062009 (2019).
19. D. Wu, Y. Zhao, and J. Li, "PCF taper-based Mach–Zehnder interferometer for refractive index sensing in a PDMS detection cell," Sens. Actuators, B **213**, 1–4 (2015).
20. Y. Liu, X. Li, Y.-n. Zhang, and Y. Zhao, "Fiber-optic sensors based on Vernier effect," Measurement **167**, 108451 (2021).
21. A. D. Gomes, H. Bartelt, and O. Frazão, "Optical Vernier effect: recent advances and developments," Laser Photonics Rev. **15**(7), 2000588 (2021).
22. Y. Jiang, Y. Yi, G. Brambilla, and P. Wang, "Ultra-high-sensitivity refractive index sensor based on dual-microfiber coupler structure with the Vernier effect," Opt. Lett. **45**(5), 1268–1271 (2020).
23. G.-T. Chen, Y.-X. Zhang, W.-G. Zhang, L.-X. Kong, X. Zhao, Y. Zhang, Z. Li, and T.-Y. Yan, "Double helix microfiber coupler enhances refractive index sensing based on Vernier effect," Opt. Fiber Technol. **54**, 102112 (2020).
24. N. F. Baharin, A. I. Azmi, A. S. Abdullah, and M. Y. Mohd Noor, "Refractive index sensor based on lateral-offset of coreless silica interferometer," Opt. Laser Technol. **99**, 396–401 (2018).
25. J. Hu, M. Smietana, T. Wang, T. Lang, L. Shao, G. Gu, X. Zhang, Y. Liu, X. Song, Z. Song, J. Feng, and R. Buczynski, "Dual Mach–Zehnder interferometer based on side-hole fiber for high-sensitivity refractive index sensing," IEEE Photonics J. **11**(6), 1–13 (2019).
26. J. Li, M. Zhang, M. Wan, C. Lin, S. Huang, C. Liu, Q. He, X. Qiu, and X. Fang, "Ultrasensitive refractive index sensor based on enhanced Vernier effect through cascaded fiber core-offset pairs," Opt. Express **28**(3), 4145–4155 (2020).
27. X.-Z. Wang and Q. Wang, "A high-birefringence microfiber Sagnac-interferometer biosensor based on the Vernier effect," Sensors **18**(12), 4114–4121 (2018).
28. F. Zhang, B. Li, Y. Sun, W. Liu, X. Yan, X. Zhang, F. Wang, S. Li, T. Suzuki, Y. Ohishi, and T. Cheng, "A magnetic field sensor utilizing tellurite fiber-induced Sagnac loop based on Faraday rotation effect and Fresnel reflection," IEEE Trans. Instrum. Meas. **70**, 1–7 (2021).
29. B. Wu, C. Zhao, B. Xu, and Y. Li, "Optical fiber hydrogen sensor with single Sagnac interferometer loop based on vernier effect," Sens. Actuators, B **255**, 3011–3016 (2018).
30. Y.-n. Zhang, L. Zhang, B. Han, P. Gao, Q. Wu, and A. Zhang, "Reflective mercury ion and temperature sensor based on a functionalized no-core fiber combined with a fiber Bragg grating," Sens. Actuators, B **272**, 331–339 (2018).
31. K. Wang, X. Dong, M. H. Kohler, P. Kienle, Q. Bian, M. Jakobi, and A. W. Koch, "Advances in optical fiber sensors based on multimode interference (MMI): a review," IEEE Sens. J. **21**(1), 132–142 (2021).
32. G. Xiao, K. Zhang, Y. Yang, H. Yang, L. Guo, J. Li, and L. Yuan, "Graphene oxide sensitized no-core fiber step-index distribution sucrose sensor," Photonics **7**(4), 101–114 (2020).
33. L.-Y. Shao, Y. Luo, Z. Zhang, X. Zou, B. Luo, W. Pan, and L. Yan, "Sensitivity-enhanced temperature sensor with cascaded fiber optic Sagnac interferometers based on Vernier-effect," Opt. Commun. **336**, 73–76 (2015).
34. T. Hu, Y. Zhao, and L. Cai, "Temperature and refractive index sensor using a high-birefringence fiber loop mirror and single mode-coreless-single mode fiber structure," Instrum. Sci. Technol. **44**(4), 366–376 (2016).
35. X. Li, S. C. Warren-Smith, H. Ebendorff-Heidepriem, Y.-n. Zhang, and L. V. Nguyen, "Optical fiber refractive index sensor with low detection limit and large dynamic range using a hybrid fiber interferometer," J. Lightwave Technol. **37**(13), 1 (2019).